Numerical Modeling of Groundwater-Driven Sand Infiltration into Defective Sewer Pipes using CFD-DEM

Ahmed Ibrahim & Mohamed A. Meguid
Department of Civil Engineering – McGill University, Montreal, Québec, Canada

ABSTRACT

Cracks and defects can happen in sewer pipes for various reasons such as aging, existence of chemically aggressive compounds in soil or ground movement. For pipes buried in cohesionless soils (e.g., sand), if the developed cracks are large enough, the surrounding soil may start infiltrating into the pipe. The erosion of sand into the pipe can be further accelerated in the presence of groundwater table due to the additional momentum provided by the water flow through the cracks. As these dynamics may go undetected, large cavities and sinkholes can develop when a large quantity of sand is eroded, which may compromise the integrity of the nearby buried utilities and structures. In this study, we use coupled Computational Fluid Dynamics-Discrete Element Method (CFD-DEM) to resolve the complex interactions of sand-water flow around pipe cracks. Focusing on the factors affecting the erosion rate and extent, a parametric study was carried out to examine the effect of groundwater table, crack width, crack angle and the height of sand layer above the pipe. It was found that the erosion process is accelerated with increasing the groundwater level, however, only to a certain extent, beyond which, it remains constant. The results of this numerical study will allow for better understanding of the process of soil erosion into defective pipes.

RÉSUMÉ

Les fissures et les défauts peuvent survenir dans les tuyaux d'égouts pour différentes raisons telles que le vieillissement ou la présence de substances chimiques agressives dans le sol avoisinant. Dans le cas où un tuyau possédant de larges fissures est enfoui dans un sol sans cohésion (ex : sable), le sol peut s'infiltrer à l'intérieur de ce dernier. L'érosion du sable dans le tuyau peut être accélérée par la présence d'une nappe phréatique à cause de la quantité de mouvement additionnelle apportée par l'eau lorsqu'elle passe dans les fissures. Comme ces effets dynamiques peuvent se produire sans être détectés, de grandes cavités et des dolines peuvent apparaitre quand une quantité de sable suffisante est érodée, posant ainsi un risque pour les structures souterraines se trouvant aux alentours. Dans cette étude, la mécanique des fluides numérique couplée avec la méthode des éléments discrets sont utilisées pour décrire les interactions complexes du flux de sable et d'eau autour de fissures dans un tuyau. Une étude paramétrique se concentrant sur les facteurs qui influence le taux et l'ampleur de l'érosion est entreprise pour étudier les effets de la nappe phréatique, largeur des fissures, angle des fissures, et de la hauteur de la couche de sable qui repose au-dessus du tuyau. Les résultats indiquent que le processus d'érosion est accéléré par le niveau de la nappe phréatique seulement jusqu'à un certain point après quoi le taux d'érosion devient constat. Les résultats de cette étude aideront à mieux comprendre le processus d'érosion du sol dans les tuyaux fissurés.

1   INTRODUCTION

Cracks and defects can happen in sewer pipes for various reasons such as aging, existence of chemically aggressive compounds in soil or ground movement. For pipes buried in cohesionless soils (e.g., sand), if the developed cracks are large enough, the surrounding soil may start infiltrating into the pipe. The erosion of sand into the pipe can be further accelerated in the presence of groundwater table due to the additional momentum provided by the water flow through the cracks. As these dynamics may go undetected, large cavities and sinkholes can develop when a large quantity of sand is eroded, which may compromise the integrity of the nearby buried utilities and structures.

A few studies presented numerical investigation and simplified analytical solution for the flow of soil-water mixtures around sewer pipes. Guo and Zhu (2017) presented a simplified formulation for the flow of sand and water based on the freefall arch theory (Beverloo et al., 1961). That is, the flow of sand particles into the vicinity is governed by a temporary arch or hemisphere, in which, the particles fall solely under the effect of gravity. In their work, the freefall arch theory was developed such that it accommodates the additional drag and buoyancy forces exerted by the fluid. More recently, Qian et al. (2021) presented a coupled Computational Fluid Dynamics-Discrete Element Method (CFD-DEM) simulation of the migration of fine particles through defects in segmented tunnels. In CFD-DEM simulation, the sand grains are generally represented as individual particles for which the movement and trajectory are determined by resolving the coupling of interparticle forces from DEM and particle-fluid interaction forces from CFD (Ibrahim and Meguid, 2020; Zhu et al., 2007). This is particularly challenging because it is computationally expensive to track such large number of particles and resolve the complex physics of soil-water interaction at the microscale level. Some simpler continuum-based models have been used in similar context such as simulating internal erosion around pressurized pipes (Ibrahim and Meguid, 2021; Salimi-Tarazouj et al., 2021; Tang et al., 2017a). Nonetheless, with the smoothing technique followed in these models,

intricate interaction such as the formation of the freefall arch cannot be captured. Thus, residing to discrete particulate modeling as the case in CFD-DEM or Smoothed Particle Hydrodynamics (SPH-DEM) is necessary to understand the mechanism of erosion initiation and evolution as well as its sensitivity to different parameters.

In this study, we use coupled Computational Fluid Dynamics-Discrete Element Method (CFD-DEM) to resolve the complex interactions of sand-water flow around pipe cracks. Focusing on the factors affecting the erosion rate and extent, a parametric study was carried out to examine the effect of groundwater table, crack width, crack angle and the height of sand layer above the pipe.

2   NUMERICAL ANALYSIS

The governing equations for the fluid phase consist of the volume-averaged continuity and Navier-Stokes equations (Anderson and Jackson, 1967; Kloss et al., 2012)

$$\frac{\partial \alpha_f}{\partial t} + \nabla \cdot \left(\alpha_f \mathbf{u}_f \right) = 0 \tag{1}$$

$$\frac{\partial \left(\alpha_f \mathbf{u}_f \right)}{\partial t} + \nabla \cdot \left(\alpha_f \mathbf{u}_f \mathbf{u}_f \right) = -\alpha_f \nabla \frac{p}{\rho_f} - \mathbf{R}_{pf} + \nabla \cdot \boldsymbol{\tau} \tag{2}$$

where α_f is the volume fraction of the fluid (e.g., water) within a computational cell, $\mathbf{u}_f$ is the fluid velocity, p is the fluid pressure, $\boldsymbol{\tau}$ is the volume-average shear stress tensor of the fluid, ρ_f is the density of the fluid, and $\mathbf{R}_{pf}$ is a term for momentum transfer between the solid and fluid phases (i.e., particle-fluid interaction force). For the solid phase, the governing equations of Discrete Element Analysis (DE) are given as:

$$m_i \frac{d\mathbf{v}_i}{dt} = \sum_{j=1}^{k_c} \left(\mathbf{f}_{i,n} + \mathbf{f}_{i,t} \right) + \mathbf{f}_{i,b} + \mathbf{f}_{i,pf}$$

$$I_i \frac{d\boldsymbol{\omega}_i}{dt} = \sum_{j=1}^{k_c} \mathbf{r}_{ij} \times \mathbf{f}_{i,t} + \mathbf{M}_{i,r}$$

where m_i, I_i and $\mathbf{v}_i$ are the mass and moment of inertia particle i, respectively, $\mathbf{v}_i$ and $\boldsymbol{\omega}_i$ are its linear and angular velocities , respectively, $\mathbf{f}_{i,n}$ and $\mathbf{f}_{i,t}$ are the normal and tangential contact forces at contact points of particle i with neighboring particles, k_c is the number of neighboring particles, $\mathbf{f}_{i,b}$ is the weight and external body forces acting on particle i, $\mathbf{f}_{i,pf}$ is the interaction force exerted by the solid particle on the fluid, $\mathbf{r}_{ij}$ is the relative position vector between particle i and a neighboring particle j, and $\mathbf{M}_{i,r}$ is the additional moment exerted on the solid particle (e.g., rolling friction).

3   SIMULATION SETUP

The Simulation setup shown in Fig. 1 consists of a box with a pipe attached at the bottom. The box is filled with sand up to a height of h_s that is submerged under a water height of h_w. For three inclination angles: $\theta = 90^\circ$, $\theta = 45^\circ$, and $\theta = 0^\circ$ measured from the horizontal, a rectangular slot/opening of width D is placed. As the simulation starts, the seal on the slot is removed and sand and water are allowed to flow through the opening. Sand and water velocities within the sand bed are mapped throughout the simulation. In addition, the flowrates of water and sand through the outlet are recorded as well as the final deformation of the sand bed after all the water had moved out of the system.

4   MODEL VALIDATION

The validation case carried out in this study is a reproduction of the experimental study of Tang et al. (2017b) similar to that shown in Fig. 1. As the experiment starts, the discharge of sand and water is directed through a ramp-like outlet that represents the slope of a sewer pipe as well as to prevent clogging within the interior of the pipe. Sand and water velocities within the sand bed are mapped throughout the experiment. In addition, the flowrates of water and sand through the outlet are recorded as well as the final deformation of the sand bed after all the water had moved out of the system. The output of the experiment is useful in validating the numerical model developed in this study as it provides important insights on the mobilization, rate and the final extent of erosion.
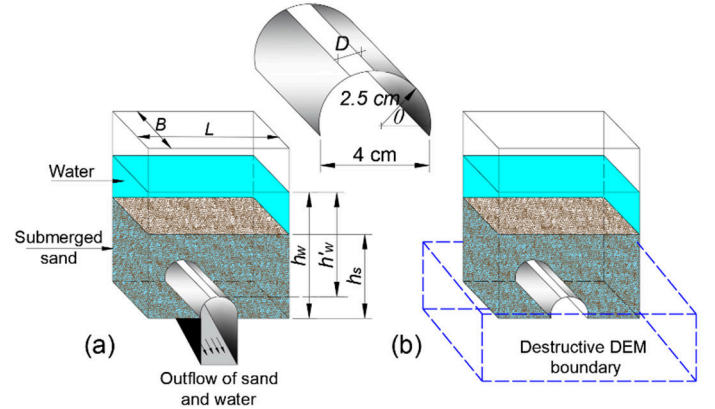

Figure 1. A schematic illustration of the simulated system

As we consider a longitudinal crack, that is only defined by its width, the resulting surface void from sand erosion is a rectangular prism as opposed to a conical void resulting from circular cracks. As far as numerical modeling is concerned, this gives us the advantage of further reducing the computational load by considering the problem to be essentially two-dimensional. From a broader view point, fundamental difference exists between the numerical model and the experiment when it comes to the variations in water level. While it is experimentally preferable to use a finite volume of water, it hardly represents the lateral extent of groundwater, which is generally much larger than the depth at which the pipe is buried. Thus, one should not expect the groundwater level to drop as quickly as it does in a finite small box, which makes considering a constant water level more realistic. On the other hand, numerically using a constant water level reduces the complexity of implementing interface-capturing calculations to account for the movement of the water surface. Subsequently, comparison between the coupled CFD-DEM and the

experimental results will only be meaningful at early times where the water level is comparable to its initial value. Therefore, the comparison is limited to the first 10 seconds of the simulation to overcome discrepancies resulting from changes in water level and to keep the computational effort within an acceptable limit.

The simulation results of the sand velocity field are presented in Fig. 2. and compared with snapshots from the experiment at three different time stamps, namely, 0.08, 5, and 10 seconds. It can be seen that the extent and velocity of the mobilized core of sand are comparable to those reported by Tang et al. (2017b) at the examined times. At 0.08 seconds, a relatively stagnant zone with lower velocity than the mobilized core is found in both the experimental and numerical results. This is a result of the flow dynamics considering that the sand does not flow continuously. Instead, a submerged freefall arch develops which spontaneously creates cycles of obstruction and non-obstruction (flow) states. As such, lower sand velocity

values can be observed near the outlet at the arch stabilization (obstruction) instances. Capturing this behavior is not guaranteed to match the experiment at all time steps for it is highly probabilistic and can simply be affected by the temporal resolution at which output is obtained. This can be observed at times 5, and 10 seconds as the sand velocity obtained from the numerical analysis appears to be slightly higher than the experimental values. Another reason for this could be the lower water head above the outlet compared to the numerical simulation, which incrementally decreases as time goes by. Further comparisons with other variables such as water and sand flowrates were not considered as the temporal resolution of the experimental data is 10 seconds in average. Nonetheless, the agreement between the overall extent of the mobilized core, velocity mapping, and the extent of the eroded sand volume indicates that the model can capture the flow characteristics and deformations.
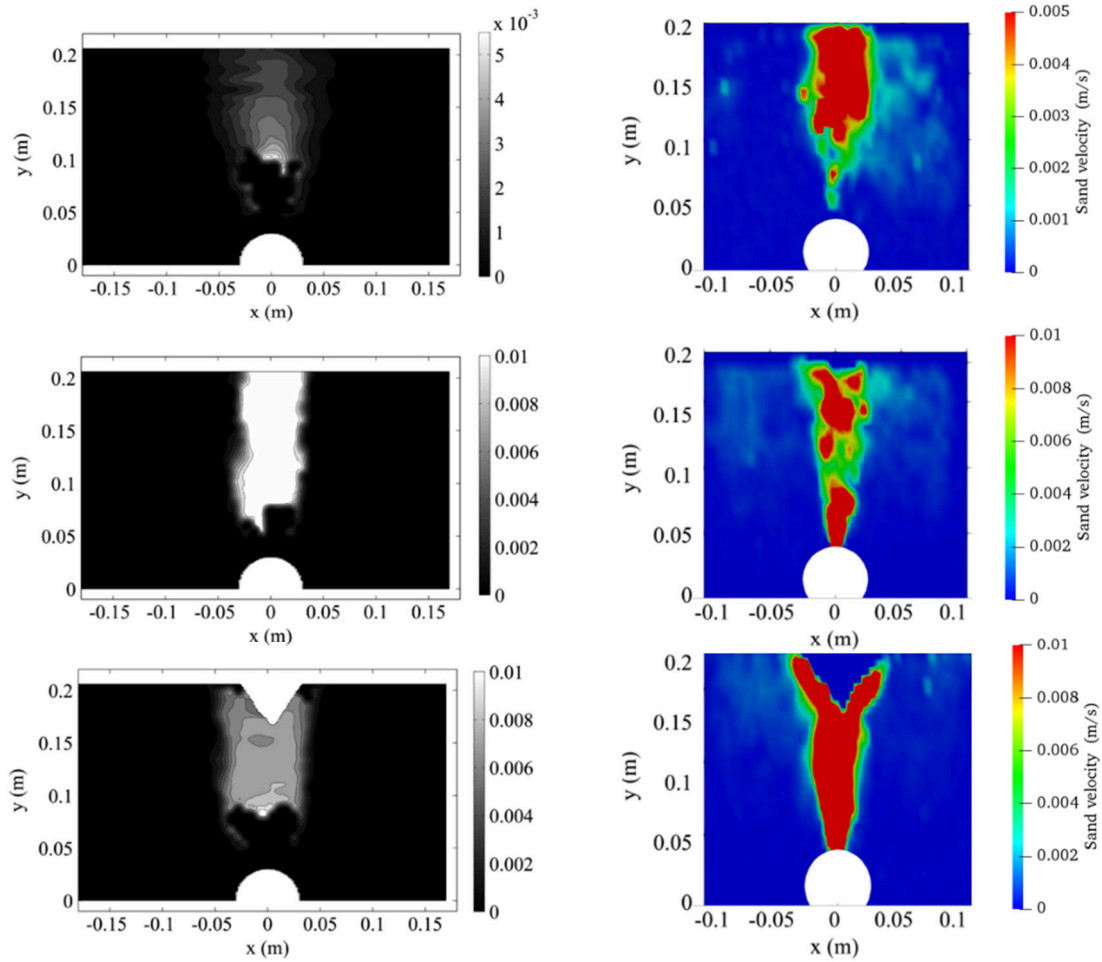

Fig. 2. A comparison between the sand velocity distribution obtained from the experiment (left) and the coupled CFD-DEM simulation (right) at times 0.08, 5 and 10 seconds.

5   RESULTS

5.1   THE EFFECT OF WATER LEVEL

The results for the cumulative eroded mass under different water levels in comparison with the dry sand case is shown in Fig. 3 for opening sizes of 9 mm and 12 mm. A basic observation is that the erosion mass rate and final eroded mass are always larger than that of dry sand. This is rather expected for the erosion rate because of the additional momentum provided by the water flow that drives the sand particles faster. Another important observation is that both the rate and total eroded mass are bound by an upper limit, referred to hereafter as the erosion plateau. Approaching this plateau value is represented in Fig. 3 by a decrease in the gap between the final eroded mass as water level increases. This implies that after reaching a certain water level both the rate and total eroded mass will not be affected by increasing the water level. This pattern appears in the 9 mm and 12 mm opening simulation cases, with a slight difference in the erosion plateau value. This could explain some of the experimental results reported in the literature such as Guo et al. (2013a). In their study, they report no significant variation in the erosion rate of sand with respect to groundwater level. However, considering the relatively large water level used in the experiment compared to the defect size, the erosion rates have most likely been in the plateau region and therefore did not display significant changes.
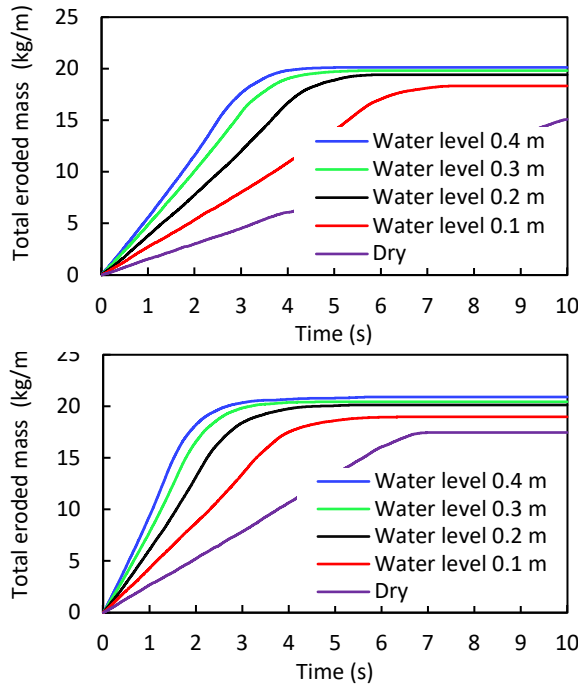
5.2   THE EFFECT OF CRACK INCLINATION

In the absence of water, the inclination of a crack, with respect to the vertical, provides a buffer against erosion as observed from pure DEM simulation. With water involved, we can extend the investigation of the rate and extent of erosion to examine mobilizing erosion in situations that would otherwise be stagnant. The simulation results shown in Fig. 4. show the propagation of erosion for different crack inclination angles under a water level of 0.2 m. It can be seen that in addition to the increase in the rate of erosion experienced compared to the dry case for $\theta = 90^o$ (Fig. 5), the erosion continued for $\theta = 45^o$ and $\theta = 0^o$ as opposed to the dry case. This is a direct result of the additional momentum contribution of water flow at the outlet which increases the kinetic energy of sand grains, and continuously disturbs the stability of the freefall arch. Furthermore, the fact that inclination angles smaller than 90° pose larger water head at the outlet provides additional energy to the flow at the outlet. With that additional energy, however, the rate of erosion for $\theta = 45^o$ and $\theta = 0^o$ is observed to remain smaller than that of $\theta = 90^o$ where the flow of sand aligns with gravity.

Further investigation of the results of cumulative eroded mass shown in Fig. 4. shows that the total eroded mass, and the correspondingly eroded volume, became larger as the inclination angle decreased. The snapshots in Fig. 5. provide a better visual of this, where the point of intersection of the final resting slope and the pipe is slightly shifted from the edge of the crack. Thus, if we assume that the final deposition angle is comparable for different inclinations, the final eroded mass and volume are always larger for inclined cracks. This provides an interesting insight that allows one to define the critical condition for sand erosion around a deteriorated pipe. That is, inclined cracks which are initially clogged in dry situations and would typically go undetected can become active and lead to large sinkholes or cavities. As one would not expect pipe cracks to always be at the pipe crown, we can fairly assume a number of clogged cracks that would only get activated upon a sudden rise in groundwater levels.
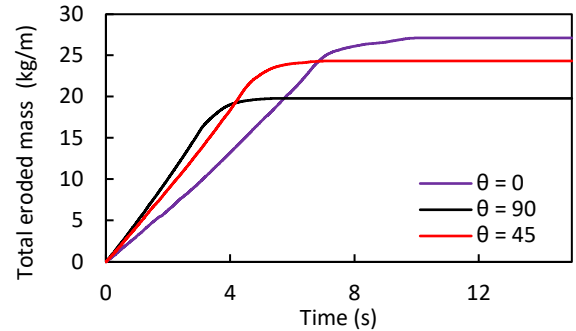

Fig. 3. Total lost mass variation with groundwater level

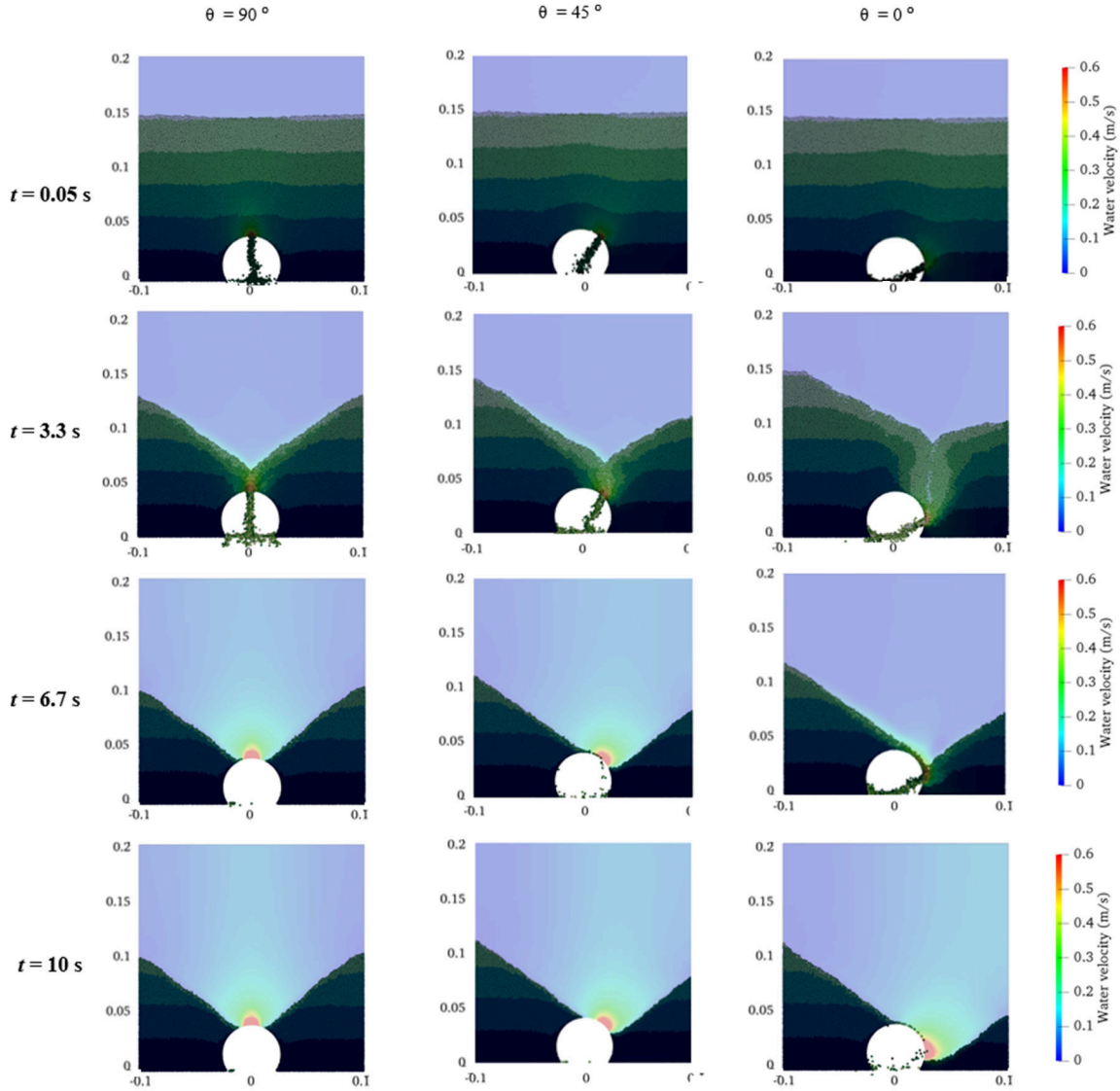
Fig. 4. Total lost mass variation with different crack angles

Fig. 5. Final sand deposition for inclined cracks at $\theta = 90°$, $\theta = 45°$, and $\theta = 0°$

5.3 THE EFFECT OF CRACK WIDTH

The simulation results for different crack widths, D, under water level of 0.2 m are shown in Fig. 6. The results show the development of a stable arch for opening sizes of 4 mm and 6 mm similar to the flow behaviour in the dry condition. For a crack width of 6 mm, however, we observe continuation of the flow up to approximately 1 second before the flow stops. The total eroded mass is nearly 160% of that estimated in the dry case, which indicates some degree of mobilization that was yet not sufficient to continue driving the erosion. For crack width of 4 mm, the erosion almost stopped immediately at the beginning of the simulation with no noticeable differences from that of the dry case. In contrast to the mobilization of sand particles observed with crack inclination, narrowing the opening size below $6d_p$ seems to eventually stop the sand erosion. One reason for this difference in mobilization could be because

of the lateral force component exerted by water when the arch is inclined that work against its stability more than that if it were vertical.

Another way to look at the issue of sand mobilization around the outlet is to examine the evolution of the kinetic energy of the system. As stated by Arevalo and Zuriguel (2016), the erosion process involves an initial avalanche that provides some kinetic energy required to help collapsing the arch formation at early times. Following that initial avalanche, if the kinetic energy of the particles in the vicinity of the outlet is sufficiently large, the erosion process will continue. Thus, a complete stoppage of erosion will be preceded by significant dissipation in the kinetic energy of the system. Here, we revisit the four "clogged" cases referred to earlier in the DEM simulation of dry sand. Fig. 7. shows the state of the sand bed in both dry and submerged cases as well as the evolution of kinetic energy over time in both cases. We observe that in the first two

clogged cases of θ = 45º and θ = 0º, the kinetic energy of the system continued to grow until a maximum value is reached near the end of the freefall arch regime before it starts decreasing as the sand deposition comes to a stable formation. In contrast, the latter two clogged cases of D = 4 mm and D = 6 mm exhibit decline in the kinetic energy of the system until completely dissipated.

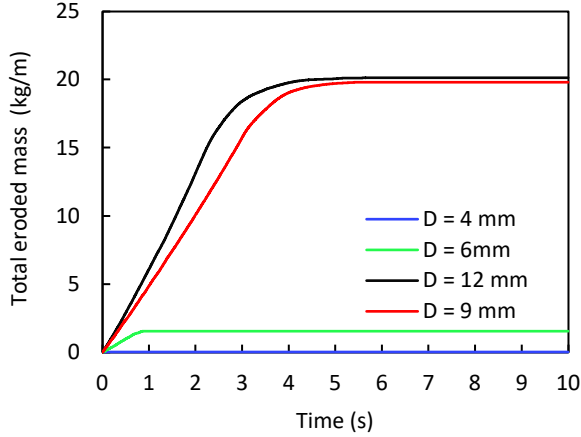Fig. 6. Total eroded mass over time for different crack widths of 4 mm, 6 mm, 9mm, and 12 mm.

5.4   THE EFFECT OF SAND LAYER THICKNESS

With explanations of the erosion phenomenon made within the context of the freefall arch, we can expect a trend similar to that of Beverlee's correlation in the case of dry sand. That is, the thickness of the sand layer will not have a significant effect on the rate of erosion until the outlet is exposed. Therefore, we conducted three different sets of simulation for three different sand thickness, namely, h_s = 0.075 m, h_s = 0.1 m, and h_s = 0.15 m, under a water level of 0.2 m and opening size of 9 mm. It can be seen from the results in Fig. 8. that for the three different layer thicknesses the erosion rate calculated was nearly equal in the freefall arch region. This confirms our hypothesis on the erosion rate following a similar, yet larger, constant flowrate to that of Beverloo. Although this observation may not agree with the models proposed by Guo et al. (2013b) and Tang et al. (2017b) where the thickness of the sand layer is among the factors that affect the erosion rate, we note that our observation only pertains to the freefall arch region as opposed to a global relationship for the erosion rate.
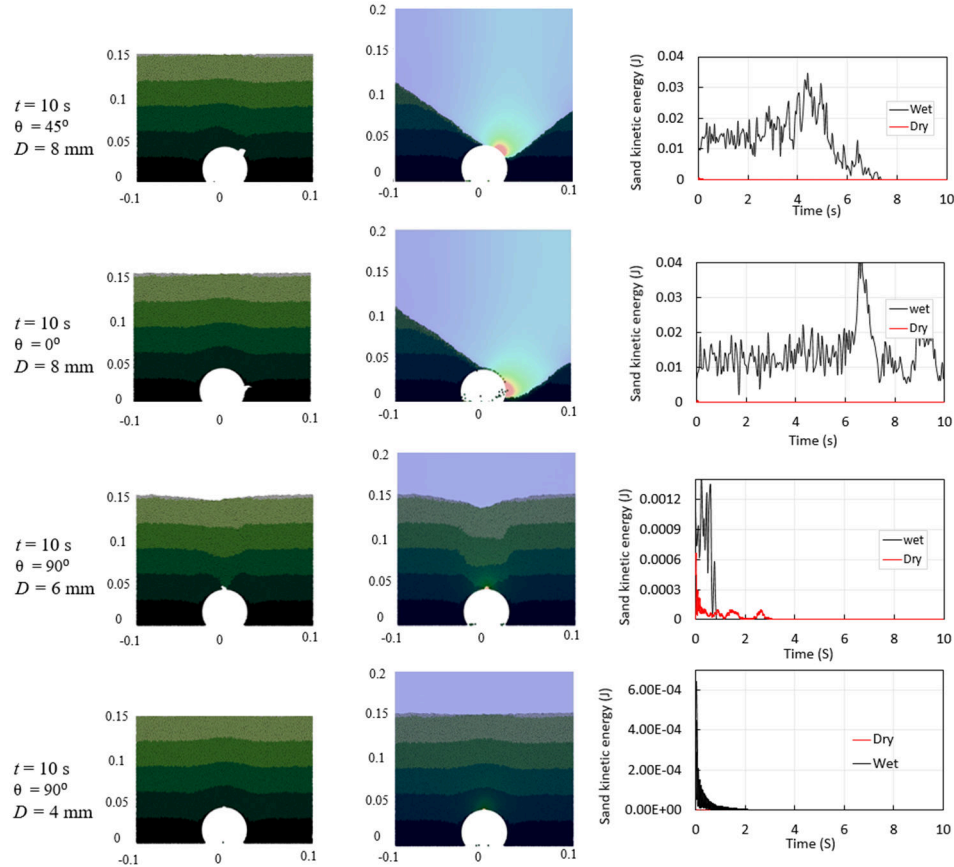

Fig. 7. A comparison between the dry and wet (hw = 0.2 m) of the four cases where a stable arch was observed along with the corresponding evolution of the kinetic energy of sand in both cases.
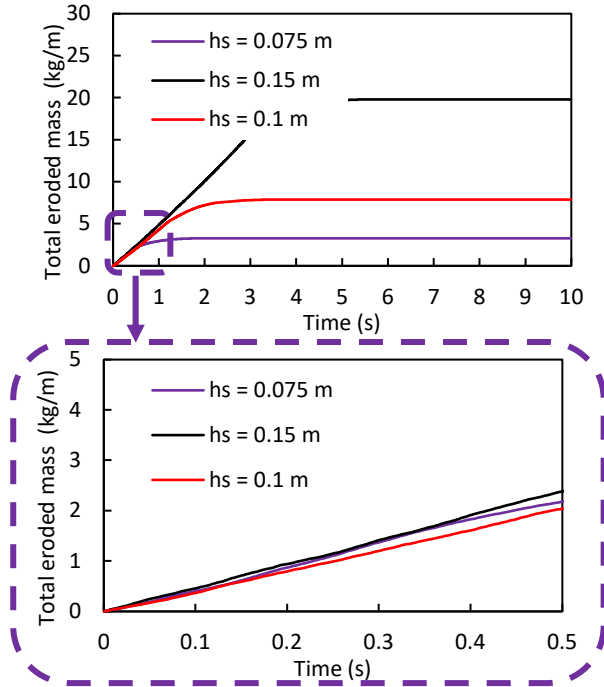
Fig. 8. The cumulative eroded mass of sand under water level 0.2 m for different sand layer height.

In addition, a key assumption to deriving their models is that Darcy flow is valid throughout the bed, which is not necessarily the case especially in the vicinity of the crack. Further experimental and numerical investigation of this issue remains necessary to provide clearer insights on the effect of sand layer thickness. In the context of our results, for real-life situations where pipes are buried at relatively larger depths, the freefall regime is most likely to be the dominant mechanism during the erosion process. As such, the erosion will only be affected by the soil properties, crack geometry, and groundwater conditions.

5   CONCLUSIONS

1- The rate and the final extent of erosion increase with increasing the water level above the pipe. However, it is shown that this increase is not indefinite but rather governed by a maximum threshold value, beyond which, increasing the water level does not affect the erosion process.

2- The final eroded mass and volume are always bounded by a lower limit that occurs when the sand is dry, and an upper limit that occurs at a certain water level, above which, no increase in the eroded volume was observed.

3- The angle of repose in all examined cases was observed to be approximately equal to that of the dry sand and was not affected by changing the water level or the inclination angle of the defect.

4- For defects inclined from the crown of the pipe, although less critical in dry cases, are likely to become active and cause larger eroded zones than defects located as the crown.

5- A freefall arch flow regime was present in both dry and submerged conditions where the erosion rate relies only on the geometry of the defect and the sand properties, where the thickness of the sand layer did not significantly affect the erosion rate in either case.

6   REFERENCES

Anderson, T.B., Jackson, R., 1967. A fluid mechanical description of fluidized bed. Equations of motion. Industrial Engineering Industry Fundamentals 6, 527-539.

Arevalo, R., Zuriguel, I., 2016. Clogging of granular materials in silos: effect of gravity and outlet size. Soft Matter 12, 123-130.

Beverloo, W.A., Leniger, H.A., Vandevelde, J., 1961. The Flow of Granular Solids through Orifices. Chemical Engineering Science 15, 260-&.

Guo, S., Shao, Y., Zhang, T.Q., Zhu, D.Z., Zhang, Y.P., 2013a. Physical Modeling on Sand Erosion around Defective Sewer Pipes under the Influence of Groundwater. Journal of Hydraulic Engineering 139, 1247-1257.

Guo, S., Zhang, T.Q., Zhang, Y.P., Zhu, D.Z., 2013b. An approximate solution for two-dimensional groundwater infiltration in sewer systems. Water Sci Technol 67, 347-352.

Guo, S., Zhu, D.Z., 2017. Soil and Groundwater Erosion Rates into a Sewer Pipe Crack. Journal of Hydraulic Engineering 143.

Ibrahim, A., Meguid, M., 2021. Continuum-Based Approach to Model Particulate Soil-Water Interaction: Model Validation and Insight into Internal Erosion. Processes 9.

Ibrahim, A., Meguid, M.A., 2020. Coupled Flow Modelling in Geotechnical and Ground Engineering: An Overview. Int J Geosynth Groun 6.

Kloss, C., Goniva, C., Hager, A., Amberger, S., Pirker, S., 2012. Models, algorithms and validation for opensource DEM and CFD-DEM. Progress in Computational Fluid Dynamics, An International Journal 12.

Qian, J.G., Li, W.Y., Yin, Z.Y., Yang, Y., 2021. Influences of buried depth and grain size distribution on seepage erosion in granular soils around tunnel by coupled CFD-DEM approach. Transp Geotech 29.

Salimi-Tarazouj, A., Hsu, T.J., Traykovski, P., Chauchat, J., 2021. Eulerian Two-Phase Model Reveals the Importance of Wave Period in Ripple Evolution and Equilibrium Geometry. J Geophys Res-Earth 126.

Tang, Y., Chan, D.H., Zhu, D.Z., 2017a. Numerical Investigation of Sand-Bed Erosion by an Upward Water Jet. Journal of Engineering Mechanics 143.

Tang, Y., Zhu, D.Z., Chan, D.H., 2017b. Experimental Study on Submerged Sand Erosion through a Slot on a Defective Pipe. Journal of Hydraulic Engineering 143.

Zhu, H.P., Zhou, Z.Y., Yang, R.Y., Yu, A.B., 2007. Discrete particle simulation of particulate systems: Theoretical developments. Chemical Engineering Science 62, 3378-3396.